Ultrafast second-harmonic generation spectroscopy of GaN thin films on sapphire

W. E. Angerer, N. Yang, and A. G. Yodh
Department of Physics and Astronomy, University of Pennsylvania, 209 South 33rd Street, Philadelphia, Pennsylvania 19104

M. A. Khan and C. J. Sun
APA Optics, Blaine, Minnesota 55449
(Received 23 June 1998)

We have performed ultrafast second-harmonic generation spectroscopy of GaN/Al_2O_3. A formalism was developed to calculate the nonlinear response of thin nonlinear films excited by an ultrashort laser source ($Ti:Al_2O_3$), and then used to extract $\chi^{(2)}_{zxx}(\omega=2\omega_o)$ and $\chi^{(2)}_{xzx}(\omega=2\omega_o)$ from our SHG measurements over a two-photon energy range of 2.6–3.4 eV. The spectra are compared to theory [J. L. P. Hughes, Y. Wang, and J. E. Sipe, Phys. Rev. B **55**, 13 630 (1997)]. A weak sub-band-gap enhancement of $\chi^{(2)}_{zxx}(\omega=2\omega_o)$ was observed at a two-photon energy of 2.80 eV; it was not present in $\chi^{(2)}_{xzx}(\omega=2\omega_o)$. The enhancement, which may result from a three-photon process involving a midgap defect state, was independent of the carrier concentration, intentional doping, and the presence of the ''yellow luminescence band'' defects. In addition, we determined sample miscuts by rotational SHG; the miscuts did not generate observable strain induced nonlinearities. The linear optical properties of GaN from 1.38 to 3.35 eV were also determined.
[S0163-1829(99)03204-X]

I. INTRODUCTION

The optical, electrical, structural, and defect properties of GaN (Refs. 2–6) are important to understand, in part, as a result of GaN's attractiveness as a material for electro-optic devices.[7] In this paper we have explored the nonlinear optical properties of GaN and its interfaces. Several second-harmonic generation (SHG) measurements of GaN (Refs. 8–12) have been reported. These works measured the nonlinear susceptibility elements of GaN at a single fundamental wavelength of 1064 nm (Refs. 8–10,12) and for two-photon energies above the band gap.[11]However, none of these measurements have probed the second-order susceptibility as a function of wavelength below the band gap. In this spectral region the contributions of defect states, such as those associated with yellow band luminescence, may be detectable.

We have measured the second-order nonlinear response of GaN over a two-photon spectral range from 2.6 to 3.4 eV in two polarization configurations, and compared these results with theory.[1] In order to extract $\chi^{(2)}_{xzx}$ and $\chi^{(2)}_{zxx}$ from the measurements, we developed an analysis that incorporates the interference effects that arise in SHG spectroscopy of thin films with ultrafast light pulses. We find the variation of these nonlinear susceptibilities to be independent of the concentration of defect states associated with yellow band luminescence. GaN shows a modest enhancement of $\chi^{(2)}_{zxx}$ at a two-photon energy of 2.80 eV. This enhancement is absent in $\chi^{(2)}_{xzx}$ and may result from point defect states with energies that lie only in the band gap. In addition, we separated the contribution of bulk and interface nonlinearities; no resonant interface states were observed in the spectral range explored. Finally, as part of these studies, we measured the linear optical properties of the GaN/Al_2O_3 samples from 370 to 900 nm and we determined a Sellmeier equation for the index of refraction of GaN.

The remainder of this paper is organized as follows. First, we present our experimental techniques and measurements of the index of refraction of GaN. Second, we discuss our photoluminescence measurements of GaN and show how our samples may be distinguished by the presence or absence of the yellow luminescence band. Third, we discuss our experimental technique for measuring and normalizing our SHG spectra from GaN. In this section, we also present a calculation of the nonlinear response of a thin slab and a thin film stack to an ultrafast laser pulse. We then apply this analysis to our quartz and GaN measurements. Finally we present and discuss our SHG spectra and symmetry measurements of GaN.

II. EXPERIMENTAL AND THEORETICAL BACKGROUND

In this section we describe sample preparation, transmission experiments to determine the linear optical properties of GaN (index of refraction), and photoluminescence experiments to probe the defect structure of GaN. We then describe our experimental apparatus for second-harmonic generation spectroscopy, and show how the nonlinear optical signals generated using an ultrafast fundamental light source depend on wave-vector mismatch and group velocity mismatch. This latter effect must be included to accurately determine the absolute value of the second-order susceptibility elements when using ultrafast pulses for nonlinear spectroscopy.

A. Samples

The procedures used to grow our samples are described in the literature.[13] Here we briefly review the procedure. A basal plane, i.e., [0001], sapphire substrate was degreased and etched in hot $H_3PO_4:H_2SO_4$. After placing the sapphire substrate onto a silicon carbide coated graphite susceptor in the reaction chamber, a 0.05-μm buffer layer of AlN was

TABLE I. Properties of GaN/Al_2O_3 samples. ''Yellow band'' refers to the observation of a yellow photoluminescence band. The uncertainty in the thickness measurements is ± 0.004 nm. The film thickness has units of μm and the mobility has units of $cm^2/V\,s$.

No.	Dopant	Thickness	Mobility	Carrier Density	Yellow band
G1984.1	none	1.020	20	4.47×10^{17}	no
G927.3	none	4.885	346	8.52×10^{17}	yes
G921.3	Si	3.765	192	2.13×10^{18}	yes

deposited by low-pressure metalorganic chemical vapor deposition (LPMOCVD). GaN films with various thicknesses were deposited using triethylgallium (TEG) and ammonia as the Ga and N sources, respectively. Some samples were intentionally *n* doped with Si using SiH_4 as a source gas. After growth, the samples were electrically characterized by Van der Pauw and Hall measurements. The results of these measurements are displayed in Table I. The sample thicknesses ranged from 1.020 to 4.885 μm.

In principle, the transmission of linear and second-harmonic light through our samples is affected by the AlN buffer layer. In this paper we determine the dispersion of both the second-order susceptibility and the index of refraction of GaN. All of our calculations model the $GaN/AlN/Al_2O_3$ layered structure as a GaN/Al_2O_3 structure. We determined the fractional error in the calculated transmitted linear and second-harmonic light that results from using the simplified two-film model in lieu of the three-film model. Our model parameters include the index of refraction of AlN,[14] the second-order susceptibility of AlN,[15] and our measured values for the index of refraction and the second-order susceptibility of GaN. The index of refraction calculated from the GaN/Al_2O_3 model has an effective random fractional error of less than 1.4% as compared with the $GaN/AlN/Al_2O_3$ model. Similarly, we calculated the fractional error in the second-order susceptibility elements using the two-slab model. This model error is less than 6%, which is about equal to our experimental uncertainty. Therefore, we implemented the two slab model for calculating the second-order susceptibilities for GaN in the experimental samples.

B. Linear optical properties

We performed a series of optical transmission measurements from 370 to 900 nm to determine the index of refraction of our GaN samples. Accurate knowledge of this parameter and of the sample thickness is essential for deriving the nonlinear susceptibility from the SHG spectra. Our dispersion relation for GaN is consistent with other measurements of the index of refraction[16,17] and shows a slightly larger value near the band gap. [We measure $n=2.613$ as compared with 2.595 (Ref. 16) and 2.589 (Ref. 17) at a wavelength of 382 nm.]

The experimental setup for our optical transmission measurement employs a 450 W Xe lamp with an f/1.0 UV enhanced lens as the light source. A monochromator selected the desired probe wavelength. The light was then *p* polarized and amplitude modulated by an optical chopper. A fraction of the light was separated and detected with a Si photodiode in order to normalize temporal fluctuations of the light source. The remaining light was transmitted through the GaN/Al_2O_3 sample and detected using a Si photodiode. At each wavelength we measured the transmission through the GaN/Al_2O_3 sample as a function of the angle of incidence from 0° to 75°. This was compared to the intensity detected with the sample removed from the optical line.

We determined a Sellmeier dispersion equation for the index of refraction of GaN from our linear transmission experiments. The transmission of light through our GaN/Al_2O_3 samples was analyzed using matrix methods[18,19] using the known linear optical properties of Al_2O_3.[20] The details of this analysis are presented in (Ref. 19). Using this theory, we fit our transmission data for the index of refraction. Figure 1 displays our data and exhibits the fits to the optical transmission of a GaN/Al_2O_3 sample. From the results we derived a two term Sellmeier dispersion relation for the index of refraction of GaN, i.e.,

$$n^2(\lambda)=1+\frac{A_1\lambda^2}{\lambda^2-\lambda_1^2}+\frac{A_2\lambda^2}{\lambda^2-\lambda_2^2}. \tag{1}$$

The parameters for this fit are listed in Table II.

Note, our transmission theory also includes the effect of a broadband light source. The wavelength intensity distribution of our light source, $I(\lambda)$, has a functional form well approximated by

$$I(\lambda)=I_o\exp\left(-\frac{8(\lambda-\lambda_o)^2}{\Delta\lambda^2}\right), \tag{2}$$

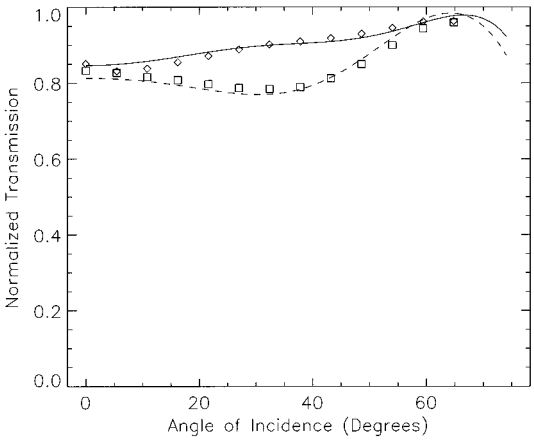

FIG. 1. Optical transmission data for GaN/Al_2O_3 with a film thickness of 1.020 μm. Transmission spectra are for $\lambda=777$ nm ($\diamond$) and $\lambda=549$ nm ($\square$). The solid (dashed) line is the best fit to the $\lambda=777$ (549) nm data using a matrix methods with a finite bandwidth light source.

TABLE II. Empirical constants for GaN Sellmeier equation. The λ_i parameters are expressed in μm.

Sellmeier constant	Value
A_1	4.081
λ_1	0.1698
A_2	0.1361
λ_2	0.3453

where λ_o is the central wavelength of the monochromator and $\Delta\lambda = 4$ nm is the wavelength bandwidth. In practice, the interference of light with a broadband spectral intensity distribution of Eq. (2) exhibits dramatically different behavior in thin and thick films. Thin films are characterized by a thickness $d \ll 2\lambda^2/n\Delta\lambda$, where n for GaN ranges from 2.32 to 2.68 over our measurement. The transmission of light through a thin film is very sensitive to the film's index of refraction and its thickness as a result of the interference of multiply reflected waves in the film. Conversely, in thick films, where $d \gg 2\lambda^2/n\Delta\lambda$, both constructive and destructive interference of the multiply reflected light occur; the light transmitted through the thick film is relatively insensitive to the film thickness and is only mildly sensitive to the index of refraction via Fresnel coefficients. For our system, GaN is a thin film ($dn\Delta\lambda/\lambda^2 < 0.2$), while sapphire is a thick film ($dn\Delta\lambda/\lambda^2 \sim 10$). This is the ideal combination for measuring the index of refraction of GaN because the transmitted intensity is highly sensitive to the index of refraction of GaN but is relatively insensitive to the optical properties of sapphire.

C. Photoluminescence measurements

To characterize the defect structure of GaN, we measured the photoluminescence spectrum of our GaN samples at 82 K. A cw krypton-ion laser optically excited electrons from the GaN valence band to the conduction band. Photoluminescent light from the GaN sample was collected with a lens and focused on the entrance slit of a single pass monochromator. The light was detected with a PMT. The monochromator slits were set to 0.25 mm to give a spectral resolution of 0.5 nm. The sample was cooled by liquid nitrogen in a dewar. As a result of the limited sensitivity of our detection system for light with wavelengths shorter than 370 nm, the band-edge features were not resolved.

Figure 2 displays photoluminescence data from our unintentionally doped 1.020-μm and 4.885-μm GaN samples. Both samples show a strong feature centered at 3.28 eV. This feature has been observed in several other low-temperature photoluminescence experiments,[21–26] and has been assigned to donor-acceptor-pair (DAP) transitions. In addition, the 4.885-μm sample has a broad feature centered at 2.2 eV, which is commonly called the yellow band. This band has been observed in the photoluminescence of both bulk and epitaxial layers of GaN grown by a variety of methods. Recent theoretical[27] and experimental work[28,29] suggests that this feature may be related to transitions between a shallow donor and a compensation center or between the conduction band and a compensation center. Neugebauer and Van de Walle[27] have suggested the gallium vacancy V_{Ga} as the most likely candidate for this defect state.

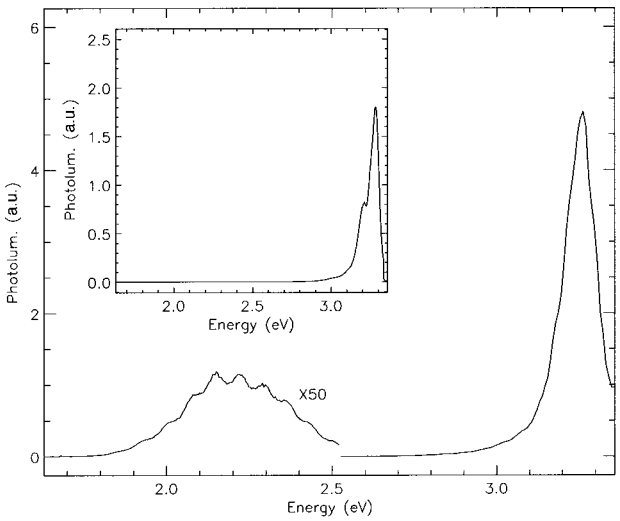

FIG. 2. Photoluminescence spectra from the unintentionally doped 4.885-μm sample. The salient features include a donor-acceptor-pair (DAP) recombination peak centered at 3.28 eV and a broad yellow luminescence band centered at 2.2 eV. The inset displays the photoluminescence spectra of our 1.020 μm sample. The DAP peak is present in this sample, but the yellow luminescence band is absent.

D. SHG experiments

We performed SHG spectroscopy and SHG rotational measurements of our GaN samples using the experimental setup displayed in Fig. 3. The fundamental light generating source is a Ti:Al_2O_3 laser. This laser produces ultrashort near IR laser pulses (700–1000 nm) at a rate of 76 MHz. These ultrashort pulses have a time duration of 80–150 fs and a peak power of $\sim$50 kW. The fundamental light from the Ti:Al_2O_3 laser was polarized and amplitude modulated with

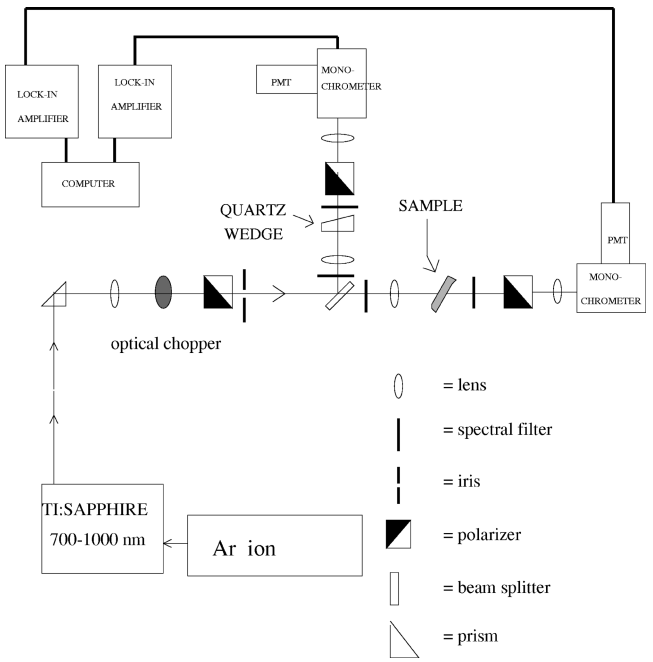

FIG. 3. Experimental setup for second-harmonic generation spectroscopy of GaN.

an optical chopper. A 90%/10% beam splitter directed the fundamental light to sample and reference arms containing identical optics. The reference line contained a plate of μ-cut quartz, which was used to normalize any spectral and temporal fluctuations of the fundamental source. With the quartz positioned normal to the Ti:Al_2O_3 beam, the fundamental light coupled to $\chi^{(2)}_{xxx}(\omega=2\omega_o)$, and the second-harmonic fields propagated through the crystal free of the effects of optical activity or birefringence.[30] A long pass filter removed any second-harmonic signal generated in the optical line prior to the sample. Achromatic lenses focussed the Ti:Al_2O_3 laser light to a spot size of ~ 100 μm on the GaN/Al_2O_3 sample and on the quartz plate. The resulting second-harmonic light was polarized and separated from the fundamental light by short pass filters and a monochromator. The SHG light was detected by a photomultiplier tube, measured by a lock-in amplifier, and analyzed by a computer. A typical signal from a GaN/Al_2O_3 sample with a *p*-polarized 200-mW fundamental beam was 2×10^5 photons/s.

Because SHG is so sensitive to the characteristics of the laser and detection systems, all of our SHG measurements are normalized to the nonlinear response of quartz. There are three essential features required of a properly normalized spectral measurement: minimization of the effects of temporal fluctuations of the source, compensation for the spectral variations of the source intensity and pulse width, and elimination or compensation of the inherent spectral response of the detection system. The simultaneous SHG measurements of quartz in the reference arm and GaN/Al_2O_3 in the sample arm address the first two issues. However, although the optics in both the reference and sample arms are nominally identical, identical spectral response is not ensured. We eliminated the spectral response systematics of the detectors by referencing the measured nonlinearity of GaN to an equivalent measurement of the nonlinearity of quartz, which was placed at the same position in the sample arm.

E. Analysis of SHG from an ultrafast fundamental source

Before analyzing the nonlinear spectra of GaN, it was necessary to consider several features of nonlinear optics that arise when using an ultrafast laser source, e.g., laser sources with pulse durations of ~ 100 fs. Consider for example the phenomena of Maker fringes,[31] in which the measured transmitted intensity of the SHG light emerging from a quartz plate oscillates strongly as a function of the orientation of the quartz plate with respect to the fundamental beam direction. The observed alternating maxima and minima result from interference between the bound and free second-harmonic fields. We do not observe Maker fringes from a similar quartz plate excited by our Ti:Al_2O_3 laser [see Fig. 4(a)]. Interference is suppressed because the bound and free wave packets[32,33] propagate through the crystal with different group velocities. Group velocity mismatch between the bound and free waves leads to incomplete overlap between the bound and free wave packets, and hence modifies the interference of these waves. Similar effects occur in our GaN samples.

We developed a formalism to analyze second-harmonic generation from an ultrafast fundamental light source. We apply these techniques to the second-harmonic light transmitted through our reference quartz slab and show that Maker fringes are absent in this material. In addition, we must apply this theory to our spectroscopic measurements of GaN. GaN is highly dispersive, and group velocity dispersion significantly affects SHG spectroscopy of our thicker samples. Our ultrafast analysis was necessary to deduce $\chi^{(2)}_{zxx}$ and $\chi^{(2)}_{xzx}$ from our raw spectroscopic data. Note that while nonlinear ultrafast pulse propagation has been addressed by several groups, particularly with regard to SHG conversion efficiency,[34–38] our treatment here is important because it explicitly considers how ultrafast pulses affect the measured nonlinearity in a spectroscopic measurement.

For our analysis we measured our laser pulse source spectral intensity, $I(\omega)$, and found that it had an approximate Gaussian angular frequency distribution, i.e.,

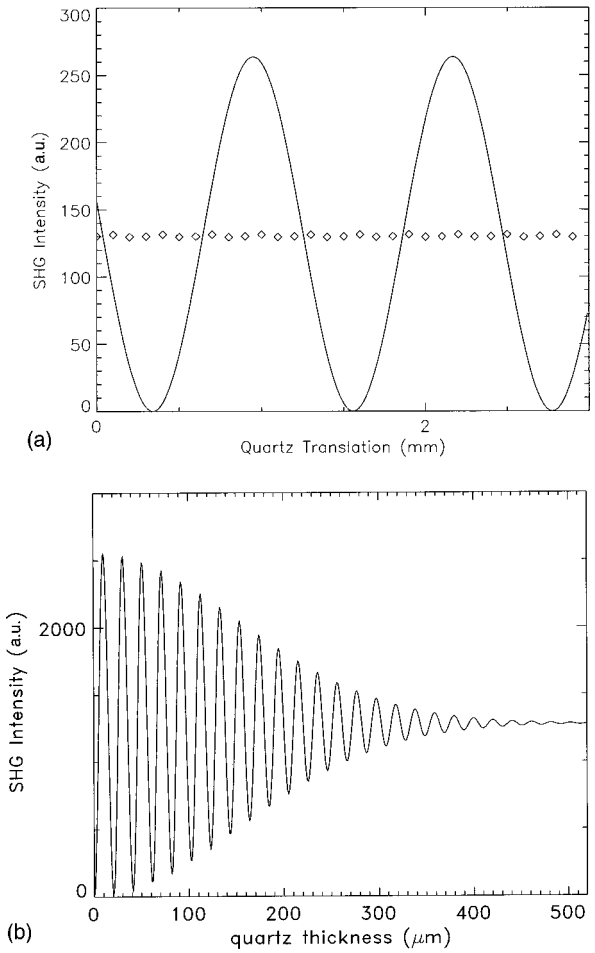

FIG. 4. (a) Comparison of SHG data from a quartz wedge excited by a Ti:Al_2O_3 laser ($\diamond$) and calculated SHG using a monochromatic theory (solid line). The quartz wedge is 3 mm thick and has faces that are aligned 1° from parallel. The Ti:Al_2O_3 pulse travels through a quartz thickness that varies as the quartz is translated perpendicularly to the beam. The calculated response displays oscillations (Maker fringes) that result from variations of the interference between the bound and free waves as the quartz thickness changes. The fundamental wavelength is 800 nm. (b) Calculated transmitted SHG intensity from a quartz slab excited by an ultrafast Ti:Al_2O_3 laser. The Maker fringes are damped as the crystal becomes thicker due to the incomplete overlap of the bound and free wave pulses (group velocity mismatch).

$$I(\omega)=I_o\exp\left(\frac{-8(\omega-\omega_o)^2}{\Delta\omega^2}\right), \tag{3}$$

where ω_o is the center angular frequency and $\Delta\omega$ is the angular frequency bandwidth, which can range from 0.021 to 0.053 fs^{-1} for our system. The electric field of a pulse propagating in the y direction and polarized along the x direction then has the form

$$\mathbf{E}(\mathbf{r},\omega)=\hat{x}\mathcal{E}e^{ik(\omega)y}\exp\left(\frac{-4(\omega-\omega_o)^2}{\Delta\omega^2}\right). \tag{4}$$

The time evolution of the pulse is obtained by Fourier transforming $\mathbf{E}(\mathbf{r},\omega)$. To facilitate these calculations, we Taylor expand the wave vector k about its central frequency ω_o, i.e.,

$$k(\omega)\approx\frac{n(\omega_o)\omega_o}{c}+\frac{(\omega-\omega_o)}{v_g}+\frac{(\omega-\omega_o)^2}{2}\left.\frac{\partial^2k(\omega)}{\partial\omega^2}\right|_{\omega_o} \tag{5}$$

with

$$\frac{1}{v_g}=\left.\frac{\partial k(\omega)}{\partial\omega}\right|_{\omega_o}. \tag{6}$$

v_g is the group velocity of the packet. The first term gives the phase velocity of the wave, the second term depends on the velocity at which the pulse propagates, and the third term accounts for pulse broadening.

Suppose our laser pulse is incident on a quartz slab of thickness d. We determine the nonlinear fields within the quartz by applying boundary conditions[32] at each angular frequency (see Appendix A for more details). The free and bound wave second-harmonic fields propagating through the quartz are expressed as

$$\mathbf{E}_j(\mathbf{r},\omega)=\hat{x}\mathsf{E}(k(\omega))e^{ik_j(\omega)y}\exp\left(\frac{-2(\omega-2\omega_o)^2}{\Delta\omega^2}\right), \tag{7}$$

where j is either b or f, denoting bound or free wave, respectively, and $\mathsf{E}(k(\omega))$ depends primarily on boundary conditions at the various interfaces.

The SHG intensity measured in transmission through the quartz film is simplified by expanding the wave vector coefficients, $\mathsf{E}(k(\omega))$, to zeroth-order in $(\omega-2\omega_o)$, and by expanding the wave-vector phases, $e^{ik_j(\omega)y}$, to first-order in $(\omega-2\omega_o)$. In other words, we approximate any wavevector that appears as a multiplicative coefficient of the field amplitude by its value at the central angular frequency, $2\omega_o$. In the case of SHG, we thus have

$$\mathsf{E}(k(\omega))\approx\mathsf{E}(k(2\omega_o)). \tag{8}$$

Bound and free wave vectors in the field phase factors, however, are written as

$$k_b(\omega)\approx\frac{n(\omega_o)2\omega_o}{c}+\frac{(\omega-2\omega_o)}{v_b} \tag{9}$$

and

$$k_f(\omega)\approx\frac{n(2\omega_o)2\omega_o}{c}+\frac{(\omega-2\omega_o)}{v_f} \tag{10}$$

with

$$v_b=\left.\frac{\partial k(\omega)}{\partial\omega}\right|_{\omega_o}\quad\text{and}\quad v_f=\left.\frac{\partial k(\omega)}{\partial\omega}\right|_{2\omega_o}. \tag{11}$$

The zeroth-order terms with respect to $(\omega-2\omega_o)$ in Eqs. (9) and (10) lead to wave-vector mismatch and the familiar Maker fringes, while the first-order terms generate a group velocity mismatch and damp the Maker fringes.

The nonlinear wave equation for the transmitted SHG intensity through quartz leads to the following expression for the temporal variation of the SHG intensity:

$$I(t)=\frac{c}{8\pi}\left[C_1^2+C_2^2+2C_1C_2\cos\left(\frac{2\omega_o}{c}(n_f-n_b)d\right)\right] \tag{12}$$

with

$$C_1=\frac{\Delta\omega^2\pi^2}{\sqrt{2}(\epsilon_b-\epsilon_f)}\mathcal{E}^2\chi^{(2)}_{xxx}(\omega=2\omega_o)\alpha\exp\left[\frac{-\Delta\omega^2}{8}\left(t-\frac{d}{v_f}\right)^2\right] \tag{13}$$

and

$$C_2=\frac{\Delta\omega^2\pi^2}{\sqrt{2}(\epsilon_b-\epsilon_f)}\mathcal{E}^2\chi^{(2)}_{xxx}(\omega=2\omega_o)\beta\exp\left[\frac{-\Delta\omega^2}{8}\left(t-\frac{d}{v_b}\right)^2\right]. \tag{14}$$

In these above equations, ϵ_f and ϵ_b are the free and bound wave dielectric susceptibilities, i.e.,

$$\epsilon_b\equiv\epsilon(\omega_o)\quad\text{and}\quad\epsilon_f\equiv\epsilon(2\omega_o), \tag{15}$$

n_b and n_f are the bound and free wave indices of refraction, $\mathcal{E}$ is the fundamental field strength, and α and β are Fresnel-like coefficients that have values

$$\alpha=\frac{-2n_f(n_b+1)}{(n_f+1)^2}\quad\text{and}\quad\beta=\frac{n_b+n_f}{n_f+1}. \tag{16}$$

In the spectroscopic measurement, the detected signal is the time integral of Eq. (12):

$$I=\frac{c}{8\pi}\int_{-\infty}^{\infty}\left[C_1^2+C_2^2+2C_1C_2\cos\left(\frac{2\omega_o}{c}(n_f-n_b)d\right)\right]dt. \tag{17}$$

Consider the consequences of Eq. (17) for ultrafast SHG. C_1 and C_2 represent the amplitudes of the free and bound wave fields, respectively. The interference of these fields occurs through $2C_1C_2\cos[(2\omega_o/c)(n_f-n_b)d]$. For a monochromatic light source, $\Delta\omega=0$, the wave packets become plane waves, and the free and bound waves always interfere. With a broadband fundamental source, $\Delta\omega\neq0$ and the bound and free wave packets are temporally centered at $t=d/v_b$ and $t=d/v_f$, respectively. Increasing the length of the sample or increasing the dispersion of the material decreases the overlap of these waves, and hence suppresses the Maker fringes. Figure 4(b) displays our calculation of the SHG transmitted

TABLE III. Parameters used for ultrafast Maker fringe calculation. Note the use of ''ultrafast units.'' τ is the time duration of the Ti:Al_2O_3 pulse and λ is the wavelength of the fundamental pulse. The indices of refraction and the group velocities are calculated for the ordinary index of quartz.

Symbol	Value
c	0.3 μm/fs
λ	0.800 μm
ω_o	2.35 fs^{-1}
$\Delta\omega$	0.053 fs^{-1}
τ	80 fs
n_b	1.5384
n_f	1.5577
v_b	0.19 316 μm/fs
v_f	0.18 695 μm/fs

intensity from a quartz slab as a function of quartz thickness. The parameters for this calculation are displayed in Table III. Because our quartz sample is 3 mm thick, we are never in a regime where Maker fringes are observed during excitation by our Ti:Al_2O_3 laser.

While ultrafast pulses dramatically affect SHG from thick quartz plates, their influence on SHG from our GaN films is of intermediate importance. We define the error, σ, in the calculated ultrafast SHG intensity compared to the monochromatic theory as

$$\sigma=\sqrt{\frac{1}{N}\sum_{i=1}^{N}\frac{(I_i^{mono}-I_i^{ultra})^2}{(I_i^{mono})^2}}, \tag{18}$$

where $I_i^{mono}(I_i^{ultra})$ is the calculated SHG intensity from GaN using the monochromatic (ultrafast) theory and i labels a wavelength at which I_i^{mono} and I_i^{ultra} are evaluated. For our 4.885-μm GaN sample, $\sigma=0.35$ over a fundamental wavelength range of 740–755 nm. The error between the monochromatic and ultrafast theories is especially large in this region due to the thickness of the sample and the high dispersion of GaN at the second-harmonic wavelength of 370–378 nm. This error is much greater than the statistical and systematic errors in our measurements. Therefore, an ultrafast analysis of SHG from GaN is required to accurately extract the nonlinear susceptibilities from our spectroscopic data.

In order to extract the wavelength dependent nonlinear susceptibilities, we compared our measurements to theoretical formulas derived using ultrafast analysis and boundary value techniques. The formulas depend on the linear and nonlinear optical properties of GaN and sapphire, as well as the angle of incidence of the fundamental field, θ_0, and the fundamental and second-harmonic field polarizations. We computed the solution in terms of monochromatic fields and then modified these solutions to include ultrafast effects. Figure 5 displays the geometry of our GaN/Al_2O_3 sample and labels the incident and the nonlinear fields. Our model relates the measured second-harmonic field to the SHG field initially created and transmitted through the GaN film, and to the SHG field that undergoes one multiple reflection in the GaN film prior to transmission through the GaN/Al_2O_3 interface. Respectively, these fields are illustrated in Fig. 5 as the fields that propagate from point A to point B and from point A to point C. The full derivation of the transmitted second-harmonic field is provided in Appendix B.

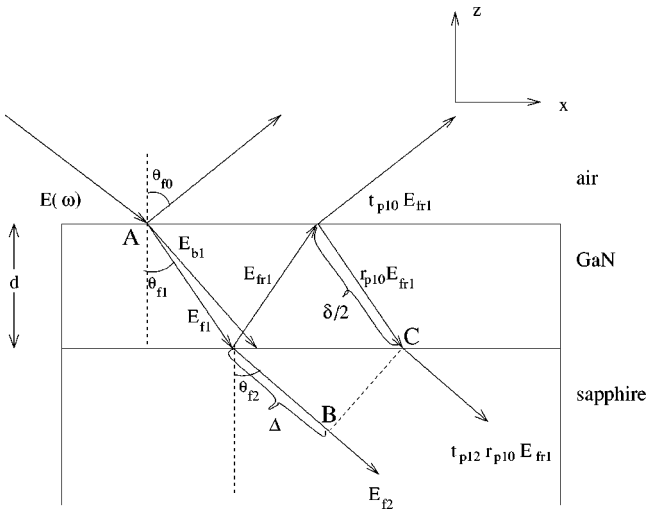

FIG. 5. Geometry of nonlinear waves in GaN/Al_2O_3. E_b is the bound wave. E_{f1} is the free wave that is generated at the air/GaN interface and propagates to the GaN/Al_2O_3 interface. E_{fr1} is the free wave that is generated at the GaN/sapphire interface and propagates to the air/GaN interface. E_{f2} is the free wave that is generated at and propagates away from the GaN/sapphire interface. Δ and δ are relative phases. Points A and B represent the path traversed by E_{f2} while points A and C represent the path traversed by E_{fr1}, which undergoes a single reflection in the GaN thin film before transmission through the sapphire substrate.

The key results are expressed in terms of the incident fields, the nonlinear susceptibilities, Fresnel factors, and the bound and free wave vectors given below:

$$k_{fi}=\frac{2\pi n_{fi}\omega}{c}, \tag{19}$$

$$k_{b1}=\frac{2\pi n_{b1}\omega}{c}, \tag{20}$$

$$k_{fiz}=-\cos\theta_{fi}k_{fi}, \tag{21}$$

$$k_{b1z}=-\cos\theta_{b1}k_{b1}, \tag{22}$$

$$k_{fix}=\sin\theta_{fi}k_{fi}, \tag{23}$$

$$\text{and}\quad k_{b1x}=\sin\theta_{b1}k_{b1}, \tag{24}$$

where i is equal to 0, 1, or 2 and denotes the air, GaN, and sapphire regions, respectively. The angle of incidence in region i is θ_i and is determined from θ_o by Snell's law. Also note that $n_{fi}\equiv n_i(2\omega_o)$ and $n_{b1}\equiv n_1(\omega_o)$.

The second-harmonic field for the s-in/p-out geometry is

$$\mathbf{E}_{sp}(2\omega_o)=\mathbf{Y}_{yy}\chi^{(2)}_{zyy}E_yE_y, \tag{25}$$

where

$$\mathbf{Y}_{yy}=t^2_{s01}(\omega_o)\mathcal{Y}_{12} \tag{26}$$

and

$$\mathcal{Y}_{mn}=\hat{e}\frac{4\pi t_{p20}(2\omega_o)}{(\epsilon_b-\epsilon_f)}\Bigg(\left(\frac{k_{f1}^2k_{f2z}}{k_{f1z}k_{f2}}+k_{f2}\right)^{-1}e^{ik_{f2}\Delta}\Bigg\{\mathcal{C}_m\Bigg[\left(k_{b1z}+\frac{k_{f1}^2}{k_{f1z}}\right)e^{-ik_{b1z}d}+2k_{f1}e^{-ik_{f1z}d}\left(\frac{k_{f0}^2k_{f1z}}{k_{f0z}k_{f1}}-k_{f1}\right)^{-1}\left(k_{b1z}-\frac{k_{f0}^2}{k_{f0z}}\right)\Bigg]$$
$$+\mathcal{C}_n\Bigg[-k_{b1x}e^{-ik_{b1z}d}-2k_{f1}k_{b1x}e^{-ik_{f1z}d}\left(\frac{k_{f0}^2k_{f1z}}{k_{f0z}k_{f1}}-k_{f1}\right)^{-1}\Bigg]\Bigg\}-r_{p10}(2\omega_o)t_{p12}(2\omega_o)e^{ik_{f1}\delta}\left(\frac{k_{f2}^2k_{f1z}}{k_{f2z}k_{f1}}+k_{f1}\right)^{-1}$$
$$\times\Bigg\{\mathcal{C}_m\Bigg[\left(k_{b1z}-\frac{k_{f2}^2}{k_{f2z}}\right)e^{-ik_{b1z}d}+e^{-ik_{f1z}d}\left(k_{f1}-\frac{k_{f2}^2k_{f1z}}{k_{f2z}k_{f1}}\right)\left(\frac{k_{f0}^2k_{f1z}}{k_{f0z}k_{f1}}-k_{f1}\right)^{-1}\left(k_{b1z}-\frac{k_{f0}^2}{k_{f0z}}\right)\Bigg]$$
$$+\mathcal{C}_n\Bigg[-k_{b1x}e^{-ik_{b1z}d}-k_{b1x}e^{-ik_{f1z}d}\left(k_{f1}-\frac{k_{f2}^2k_{f1z}}{k_{f2z}k_{f1}}\right)\left(\frac{k_{f0}^2k_{f1z}}{k_{f0z}k_{f1}}-k_{f1}\right)^{-1}\Bigg]\Bigg\}\Bigg). \tag{27}$$

The coupling of the fields in the medium determines $\mathcal{Y}_{mn}$ with

$$\mathcal{C}_1=-\frac{k_{b1x}k_{b1z}}{k_{f1}^2} \tag{28}$$

and

$$\mathcal{C}_2=\left(1-\frac{k_{b1z}^2}{k_{f1}^2}\right). \tag{29}$$

The phases in Eq. (27) of the wave that propagates from point A to point B and the wave that propagates from point A to point C in Fig. 5 are

$$\Delta=2d\tan\theta_{f1}\sin\theta_{f1} \tag{30}$$

and

$$\delta=\frac{2d}{\cos\theta_{f1}}, \tag{31}$$

respectively.

Equations (26) and (27) include Fresnel transmission and reflection coefficients of the fundamental and second-harmonic fields. For example, $t_{s01}(\omega_o)$ is the Fresnel transmission coefficient for s-polarized light from layer 0 to layer 1. The Fresnel reflection coefficient is denoted similarly with r substituted for t. Equation (25) explicitly displays the three factors on which the nonlinear response of the media depends. These factors are: the nonlinearity of the media, $\chi_{zyy}^{(2)}$; the applied fundamental field, E_y; and the propagation of the nonlinear fields, Y_{yy}. Note that Y_{yy} is a function only of the linear optical properties of the media and the GaN film thickness.

The second-harmonic response of GaN in the p-in/p-out geometry may be written similarly as

$$\mathbf{E}_{pp}(2\omega_o)=\mathbf{Y}_{xx}\chi_{zxx}^{(2)}E_xE_x+2\mathbf{Y}_{zx}\chi_{xzx}^{(2)}E_zE_x+\mathbf{Y}_{zz}\chi_{zzz}^{(2)}E_zE_z \tag{32}$$

with

$$\mathbf{Y}_{xx}=\mathbf{Y}_{zz}=t_{p01}^2(\omega_o)\mathcal{Y}_{12} \tag{33}$$

and

$$\mathbf{Y}_{zx}=t_{p01}^2(\omega_o)\mathcal{Y}_{21}. \tag{34}$$

The transmitted SHG wave is composed of a sum of waves that propagate through the film stack with various phase velocities. For example, we can rewrite the transmitted second-harmonic wave, $E_{sp}(2\omega_o)$, to explicitly display its phase dependence as

$$E_{sp}(2\omega_o)=D_{AB}^be^{i(k_{f2}\Delta-k_{b1z}d)}+D_{AB}^fe^{i(k_{f2}\Delta-k_{f1z}d)}$$
$$+D_{AC}^fe^{i(k_{f2}\delta-k_{b1z}d)}+D_{AC}^be^{i(k_{f2}\delta-k_{b1z}d)}. \tag{35}$$

Ultrafast effects are incorporated into the theory by expanding the wave-vector phases to first order in $(\omega-2\omega_o)$ as in Eqs. (9) and (10). Comparison of Eq. (35) with Eqs. (25)–(29) reveals that the D coefficients consist of $\chi_{zyy}^{(2)}$, E_y, Fresnel coefficients, dielectric constants, and wave vectors in air, GaN, and sapphire. D_{AB}^b corresponds to the wave that propagates from point A to point B in Fig. 5 and has a phase that depends on the bound wave vectors in GaN. The other D coefficients may be derived similarly. The time required for the D_{AB}^b and D_{AB}^f waves to propagate to point B and the D_{AC}^b and D_{AC}^f waves to propagate to point C is effectively contained in the phase of each wave (i.e., a group velocity is associated with each wave vector). We calculated this time by replacing each wave vector with the inverse of its group velocity and Fourier transforming the resulting expression. After carrying out this procedure, we see that ultrafast effects are included in the D_{AB}^b wave by multiplying each term by a Gaussian centered at the time required to propagate the wave from point A to point B, i.e.

$$D_{AB}^be^{i(k_{f2}\Delta-k_{b1z}d)}\rightarrow D_{AB}^be^{i(k_{f2}\Delta-k_{b1z}d)}$$
$$\times\exp\left[\frac{-\Delta\omega^2}{8}\left(t-\frac{\Delta}{v_{f2}}-\frac{d\cos\theta_{b1}}{v_{b1}}\right)^2\right]. \tag{36}$$

The ultrafast effects are incorporated similarly into the other D factors.

III. RESULTS

A. Rotational symmetry

Because second-harmonic generation is mediated by a third rank tensor, it is inherently more sensitive to material symmetry than linear processes.[39] By measuring second-harmonic generation as a function of the angle between the incident beam polarization and the crystal axes, we probed

TABLE IV. Azimuthal dependence of $P^{(2)}(\omega=2\omega_o)$ from GaN [0001]. E_i is defined as the ith component of the electric field in the GaN film.

Polarization	$P^{(2)}(\omega=2\omega_o)$
p in/p out	$2\chi^{(2)}_{xzx}E_x(\omega_o)E_z(\omega_o)+\chi^{(2)}_{zxx}E_x(\omega_o)E_x(\omega_o)+\chi^{(2)}_{zzz}E_z(\omega_o)E_z(\omega_o)$
p in/s out	0
s in/p out	$\chi^{(2)}_{zyy}E_y(\omega_o)E_y(\omega_o)$
s in/s out	0

the symmetry of our GaN thin films. Using this technique, we were able to measure film miscuts with an accuracy of $\sim 0.05°$.

GaN has C_{6v} (6 mm) symmetry and the following second-order nonlinear susceptibility elements in the dipole approximation:

$$\chi^{(2)}_{zzz}$$

$$\chi^{(2)}_{xzx}=\chi^{(2)}_{yzy}$$

$$\chi^{(2)}_{xxz}=\chi^{(2)}_{yyz}$$

$$\chi^{(2)}_{zxx}=\chi^{(2)}_{zyy}. \tag{37}$$

For second-harmonic generation, the last two indices are interchangeable, e.g., $\chi^{(2)}_{xzx}=\chi^{(2)}_{xxz}$. Note that our analysis considers only dipole second-order processes. Because GaN lacks inversion symmetry, higher-order multipole processes, such as electric quadrupole processes, are weaker than the dipole allowed process by at least a factor of $(ka)^2\approx 10^{-5}$, where a is the atomic spacing. In addition, our analysis does not consider any harmonics above second-harmonic generation. Third-harmonic and higher-harmonic light, if generated, is removed from our measured intensity by our monochromator.

The second-order susceptibility may be transformed from the crystal frame, where the elements are defined, to the lab frame, where the nonlinear signal is measured, according to

$$\chi^{(2),lab}_{ijk}=R(\phi)_{i\alpha}R(\phi)_{j\beta}R(\phi)_{k\gamma}\chi^{(2),crystal}_{\alpha\beta\gamma} \tag{38}$$

with

$$R=\begin{pmatrix}\cos\phi & \sin\phi & 0\\ -\sin\phi & \cos\phi & 0\\ 0 & 0 & 1\end{pmatrix}. \tag{39}$$

Note, the nonlinear polarization is related to second-order susceptibility as

$$P^{(2)}_i(\omega=2\omega_o)=\chi^{(2),lab}_{ijk}E_j(\omega_o)E_k(\omega_o), \tag{40}$$

where $E_j(\omega_o)$ and $E_k(\omega_o)$ are the fields inside GaN. Table IV displays the results of the calculations of the rotational symmetry of $P^{(2)}$ generated from GaN [0001]. For both the p-in/p-out and s-in/p-out measurements, the nonlinear polarization, and hence the SHG intensity, is rotationally invariant. SHG is dipole forbidden in the s-in/s-out and p-in/s-out polarizations. In contrast to the theoretical predictions, our p-in/p-out and s-in/p-out rotational data (see Fig. 6) show a onefold anisotropy. We incorporated a sample miscut into our theory to account for this modulation by modifying the form of the rotation matrix to

$$R=\begin{pmatrix}\cos\phi & \sin\phi & 0\\ -\sin\phi & \cos\phi & 0\\ 0 & 0 & 1\end{pmatrix}\begin{pmatrix}\cos\alpha & 0 & -\sin\alpha\\ 0 & 1 & 0\\ \sin\alpha & 0 & \cos\alpha\end{pmatrix}, \tag{41}$$

where α is the miscut angle of the film. Note, we have assumed that the GaN film is miscut in the xz plane. Because x and y are equivalent in C_{6v} symmetry, our measurement is sensitive only to the magnitude of the miscut but not the direction of the miscut. The fits to the p-in/p-out and s-in/p-out data yield a sample miscut of 0.78° and 0.82°, respectively. SHG rotational symmetry measurements in the p-in/s-out and s-in/s-out polarizations were complicated further by the sapphire birefringence[40] and were therefore not performed.

B. Spectroscopy

In this section we discuss our SHG spectra from GaN/Al_2O_3 in the s-in/p-out and p-in/p-out polarizations. From these spectra we extract $\chi^{(2)}_{zxx}$ and $\chi^{(2)}_{xzx}$, respectively. In

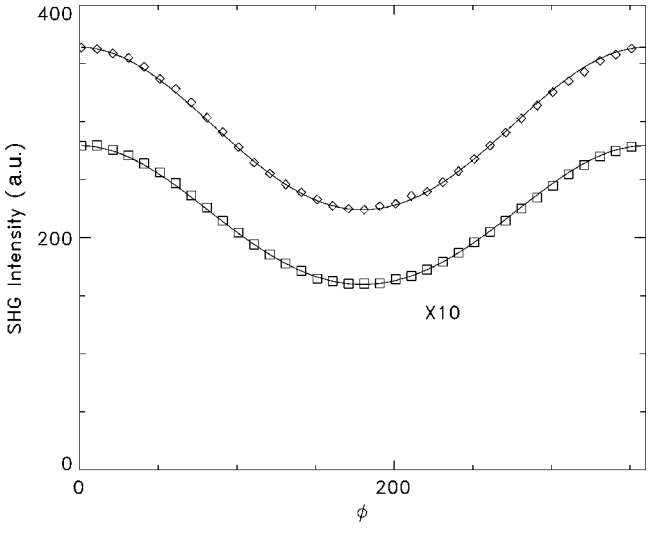

FIG. 6. Transmitted SHG intensity from GaN/Al_2O_3 as a function of crystal orientation at an angle of incidence of 15°. ϕ is the angle between the miscut direction and the plane of incidence. $\diamond$ ($\square$) is the data from the p-in/p-out(s-in/p-out) polarized second-harmonic field. The solid (dashed) line is a fit to the p-in/p-out(s-in/p-out) data with the miscut angle as a free parameter. The fitted miscut angle α is 0.78° (0.82°) for the p-in/p-out(s-in/p-out) polarizations.

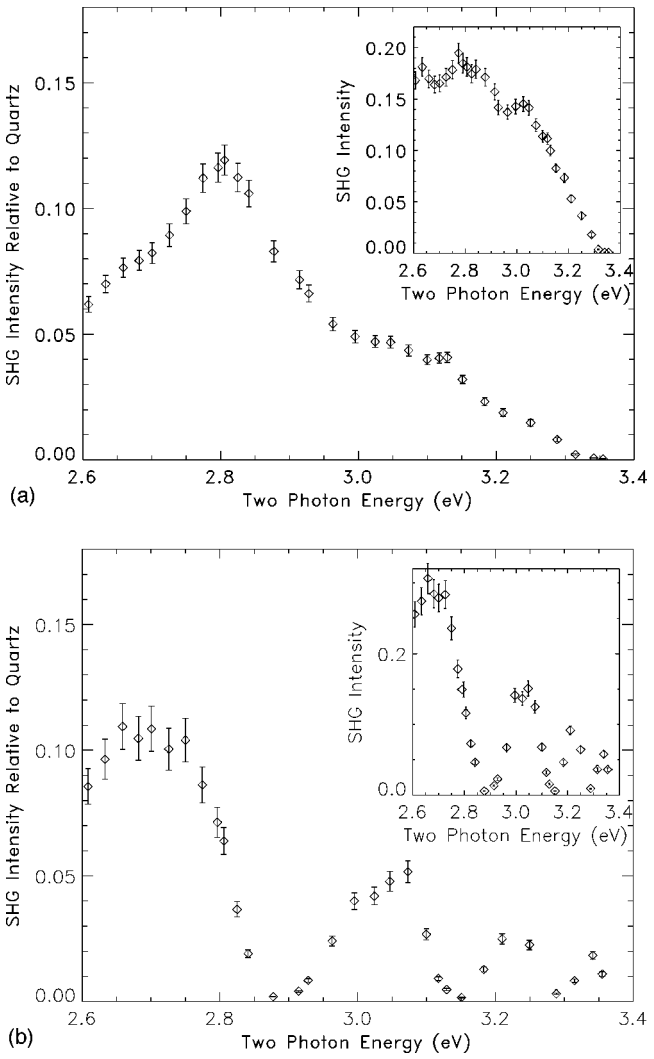

FIG. 7. (a) SHG spectroscopy from the 1.020-μm GaN sample in the s-in/p-out polarization. The inset shows SHG spectroscopy for the same sample in the p-in/p-out polarization. Both spectra are referenced to the nonlinear response of quartz in the same polarization configuration as the corresponding GaN spectra. (b) SHG spectroscopy from the 4.885-μm GaN sample in the s-in/p-out polarization. The inset shows SHG spectroscopy for the same sample in the p-in/p-out polarization. Although both samples have approximately the same nonlinear susceptibility, interference dramatically affects the transmitted second-harmonic generation intensity.

addition, from our rotational symmetry measurements as a function of the angle of incidence, we placed an upper bound on any symmetry forbidden nonlinearities, e.g., $\chi^{(2)}_{zzx}$ or $\chi^{(2)}_{xzx}$, induced by the sample miscut.

In order to accurately calculate the effects of group velocity mismatch in our GaN films, we measured $\Delta\omega$ at each wavelength by determining the wavelength distribution of the laser pulse with a monochromator. Figure 7 displays our nonlinear optical spectra from our undoped 1.020 μm and 4.885 μm GaN samples.

Using the techniques developed in the previous sections and our measured values for the linear optical properties of GaN, we extracted $\chi^{(2)}_{zxx}$ from the data. This parameter is displayed in Fig. 8. The magnitude of $\chi^{(2)}_{zxx}$ is approximately 2.4×10^{-8} esu, which is consistent with Miragliotta's average value of 2.45×10^{-8} esu measured at a single fundamental wavelength of 1064 nm.[10] This is lower than the other reported values for $|\chi^{(2)}_{zxx}|$ of 9.25×10^{-8} esu (Ref. 8) and 3.92×10^{-8} esu,[12] but is not inconsistent with the predicted value for $|\chi^{(2)}_{xzx}|=1.64\times10^{-8}$ esu.[41] The data also exhibits a weak but distinct peak centered at a two photon energy of 2.80 eV. This feature is inconsistent with the expected spectral dependence based on Miller's rule.[42]

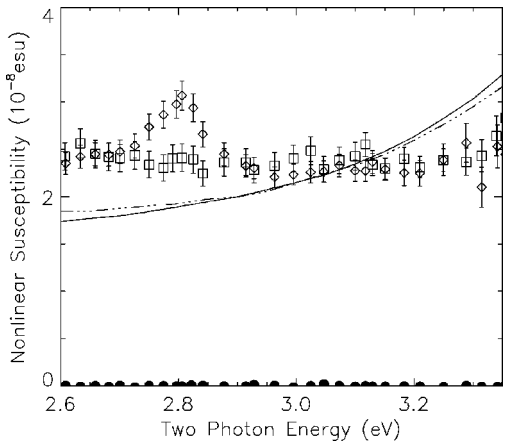

FIG. 8. Measured nonlinear susceptibility elements for GaN. $\diamond$ ($\square$) denotes $\chi^{(2)}_{zxx}(\chi^{(2)}_{xzx})$. Data represent the average values for all of the GaN/Al_2O_3 samples. The solid line (dashed) is the calculated value of $\chi^{(2)}_{zxx}(\chi^{(2)}_{xzx})$ from Ref. 1.

For measurements in the p-in/p-out polarizations, SHG couples to $\chi^{(2)}_{zzz}$ and $\chi^{(2)}_{xzx}$ in addition to $\chi^{(2)}_{zxx}$. Therefore, we measured the SHG response of GaN at several angles of incidence to fit the two unknown susceptibility elements (see Fig. 7). We observed that our spectra were very weakly dependent on $\chi^{(2)}_{zzz}$. The insensitivity of our spectra to $\chi^{(2)}_{zzz}$

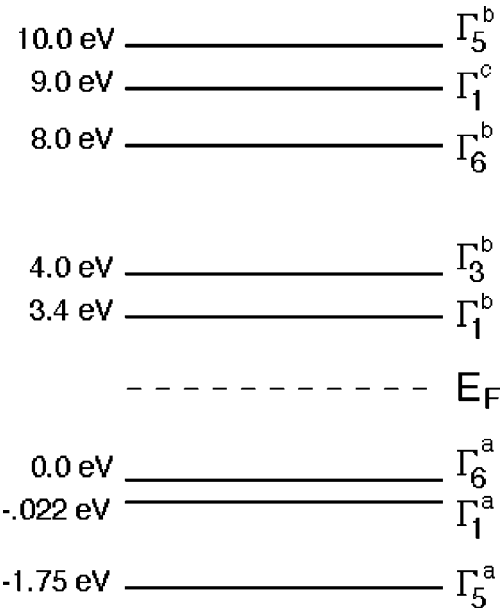

FIG. 9. Band symmetries of GaN at the Γ point. The subscript notation labels the symmetry of the band. The superscript notation is ours to distinguish between bands of the same symmetry. E_F represents the Fermi energy.

results from the fact that our nonlinear signal is proportional to $|\widehat{e_{2\omega}}\chi^{(2)}_{zzz}\widehat{e_{\omega}}\widehat{e_{\omega}}|^2 \leqslant 0.004|\chi^{(2)}_{zzz}|^2$. Therefore, we assume the theoretically predicted relationship between $\chi^{(2)}_{xzx}$ and $\chi^{(2)}_{zzz}$, i.e., $\chi^{(2)}_{zzz}=-2\chi^{(2)}_{xzx}$. Figure 8 compares the measured value of $\chi^{(2)}_{zxx}$ to $\chi^{(2)}_{xzx}$ averaged over all of our samples. Although these elements are approximately equal, as predicted by the bound charge model,[43] $\chi^{(2)}_{xzx}$ lacks a feature at a two-photon energy of 2.80 eV.

We compared our data with a theoretical calculation of the dispersion of $\chi^{(2)}_{zxx}$ and $\chi^{(2)}_{xzx}$ Ref. 1 in Fig. 8. Hughes, Wang, and Sipe[1] calculated the second-order susceptibility elements with the full-potential linearized augmented plane-wave method within the local-density approximation. The agreement between the magnitudes of the calculated and experimental second-order susceptibility elements is quite good, although the calculated data exhibits a larger dispersion in the second-order susceptibility elements than the experimental data. In addition, the calculated $\chi^{(2)}_{zxx}$ lacks a resonance at 2.80 eV. We speculate this feature may result from virtual transitions involving an intrinsic midgap defect state. Since, the calculation of the dispersion of $\chi^{(2)}_{zxx}$ includes only bulk band structures, the calculation cannot predict spectral features that couple to defect states.

By analyzing the nature of a resonance in $\chi^{(2)}_{ijk}$, the magnitude of this feature, and the symmetry of states that may participate in this resonance, we are able to make some speculative suggestions about the nature of this feature. First, we consider possible origins of the feature at a two photon energy of 2.80 eV. The second-order nonlinear susceptibility for second-harmonic generation is of the form[44]

$$\chi^{(2)}_{ijk}(\omega=2\omega_o)=-N\frac{e^3}{\hbar^2}\sum_{g,n,n'}\left[\frac{\langle g|r_i|n\rangle\langle n|r_j|n'\rangle\langle n'|r_k|g\rangle}{(\omega-\omega_{ng}+i\Gamma_{ng})(\omega_o-\omega_{n'g}+i\Gamma_{n'g})}+\cdots\right]\rho^{(0)}_g, \tag{42}$$

where N is the number of electrons per unit volume; $|g\rangle$,$|n\rangle$, and $|n'\rangle$ are states of the system, $\hbar\omega_{ng}$ is the energy difference between states n and g; Γ_{ng} is a dephasing rate; $\rho^{(0)}_g$ is the equilibrium density of the initial state g; $-er_k$ is the dipole operator along direction k; and the dots represent unique permutations of the states.

Because GaN is a direct band-gap semiconductor with a band-gap energy of 3.4 eV, the two-photon resonance at 2.80 eV cannot result from virtual transitions between valence- and conduction-band states. In addition, the requirement that the process begin with a transition between an occupied and an unoccupied state precludes any process that occurs only in the valence band or only in the conduction band. Thus, it is unlikely that the 2.80-eV feature results purely from the bulk band structure of GaN. On the other hand, it is well known that GaN is characterized by a variety of defect states.[45] The spectral feature could result from a three-photon process that involves both a defect state and the GaN bands. For example, a bulk defect state (or defect band) with energy 2.80 eV above the valence band (a midgap state) could play a role in this resonance.

A simple analysis of the $\chi^{(2)}_{zxx}$ spectrum can constrain somewhat the properties of such a defect state. We decompose the susceptibility into resonant and nonresonant terms[49] as

$$\chi^{(2)}_{zxx}(\omega=2\omega_o)=\chi^{(2)}_{zxx,res}(\omega=2\omega_o)+\chi^{(2)}_{zxx,non}=\frac{Ae^{i\phi}}{(2\omega_o-\omega_{ng}+i\Gamma_{ng})}+\chi^{(2)}_{zxx,non}, \tag{43}$$

where the symbols have the same meaning as in Eq. (42) and $e^{i\phi}$ is a phase difference between the resonant and nonresonant components. The resonant term is attributed to a two-photon resonance involving transitions to a midgap defect state and the nonresonant term is attributed to all other nonresonant bulk three-photon transitions. This decomposition assumes that the spectral dependence of $\chi^{(2)}_{zxx}(\omega=2\omega_o)$ results from the denominator of the Lorentzian term. The other terms in Eq. (43) are expected to be slowly varying functions of ω_o. Fitting this function to the data determines $\phi\approx-\pi/2$ and $\chi^{(2)}_{zxx,res}=3.8\times10^{-9}$ esu at a two-photon energy of 2.80 eV. If we assume the resonant component of $\chi^{(2)}_{zxx}$ results from defect states with a density of $N\sim10^{20}$ cm^{-3}, then the hyperpolarizability associated with these states is $\alpha_{zxx}\sim10^{-29}$ esu. This speculative analysis yields numbers that are large but not impossible.

We also determined possible three photon processes that contribute to $\chi^{(2)}_{zxx}(\omega=2\omega_o)$, but not to $\chi^{(2)}_{xzx}(\omega=2\omega_o)$, by analyzing the symmetry of the proposed midgap defect state. Defects in GaN are frequently characterized by *s*-like or *p*-like symmetry.[46] Our model assumes a defect state lies in the GaN band gap with *s*-like or *p*-like symmetry and that a three-photon process originates at either the valence band maximum or at the defect state. Group theory[47] was used to calculate the nonzero matrix elements in Eq. (42). In this calculation, we used the band symmetries determined by Bloom *et al.*[48] Figure 9 displays the symmetries of the GaN bands at the Γ point and their approximate energies. Assuming C_{6v} symmetry, *s*-like states have $A1$ (Γ_1) symmetry and *p*-like states have $E2$ (Γ_6) symmetry. Table V shows all nonzero resonant three-photon processes for $\chi^{(2)}_{zxx}(\omega=2\omega_o)$ and $\chi^{(2)}_{xzx}(\omega=2\omega_o)$. Of the cases examined, only the three-photon process that originates from a *p*-like defect state is inconsistent with our observation of a 2.80-eV resonance in $\chi^{(2)}_{zxx}(\omega=2\omega_o)$ but not in $\chi^{(2)}_{xzx}(\omega=2\omega_o)$. Figure 10 displays three-photon processes that may contribute to this resonance.

We may draw a few more qualitative conclusions from our spectroscopic data. First, the spectroscopic feature at a two-photon energy of 2.80 eV is probably not associated with yellow band defects. This conclusion results from the

TABLE V. Possible contributions to $\chi^{(2)}_{zxx}(\omega=2\omega_o)$ and $\chi^{(2)}_{xzx}(\omega=2\omega_o)$ for a defect state in the band gap of GaN. All processes are at the Γ point of the Brillouin zone. Γ_6^{defect} refers to a defect state with Γ_6 (p-like) symmetry. The labels g, n, and n' refers to the states in Eq. (42).

Susceptibility	Defect symmetry	Origin	g	n	n'
$\chi^{(2)}_{zxx}$	s like	valence	Γ_1^a	Γ_5^b	Γ_1^{defect}
$\chi^{(2)}_{zxx}$	s like	defect	Γ_1^{defect}	Γ_5^b	Γ_1^b
$\chi^{(2)}_{zxx}$	p like	valence	Γ_6^a	Γ_3^b	Γ_6^{defect}
			Γ_6^a	Γ_5^b	Γ_6^{defect}
$\chi^{(2)}_{zxx}$	p like	defect			
$\chi^{(2)}_{xzx}$	s like	valence			
$\chi^{(2)}_{xzx}$	s like	defect			
$\chi^{(2)}_{xzx}$	p like	valence			
$\chi^{(2)}_{xzx}$	p like	defect	Γ_6^{defect}	Γ_6^b	Γ_3^b

presence of the 2.80-eV feature in all samples with and without yellow band luminescence. Second, the defect is likely to be a point defect and not a defect complex. Defect complexes could arrange themselves in various bonding geometries within the lattice, and hence, the hyperpolarizabilities of the individual complexes would tend to cancel in an ensemble average. Third, several symmetries and energies may exist within the band gap of the defect state that may contribute to $\chi^{(2)}_{zxx}$ but not $\chi^{(2)}_{xzx}$, but it is impossible to determine the energy level with only SHG measurements. A possible origin of the 2.80-eV resonance may be the N_{Ga} defect state. Jenkins and Dow have predicted the N on Ga site defect state will have s-like symmetry and will lie approximately 3.0 eV above the valence band.[46] This defect state may contribute to the 2.80-eV resonance by the three photon process illustrated in Fig. 10(a).

Finally, we consider the influence of the sample miscut on possible strain-induced nonlinearities in GaN. Observation of strain and disorder effects on second-harmonic generation from vicinal $Si(111)/SiO_2$ and $Si(100)/Si_3N_4$ interfaces[50] suggests that strain-induced defect states may be generated at or near the GaN/Al_2O_3 interface. Strain is expected to couple most strongly to the components of the susceptibility elements that are perpendicular to the interface.[51] Thus, this effect may be most easily observed in $\chi^{(2),film}_{xzz}$ and $\chi^{(2),film}_{zzx}$.[52] The film superscript denotes that these elements are defined with respect to the film and not to the crystal axes, i.e., $z_{film}=z_{lab}\neq z_{crystal}$ where z_{film}, z_{lab}, and $z_{crystal}$ are the film, lab, and crystal axes. Note that these elements are defined to include only the effect of the *strain-induced nonlinearity and do not result from a coordinate transformation.* We performed rotational symmetry measurements in the p-in/p-out polarizations to probe GaN for these elements. We simplified our analysis by assuming $\chi^{(2),film}_{zzx}=\chi^{(2),film}_{xzz}$. We deduced the miscut angle of our films from the rotational symmetry data at an angle of incidence of 15° assuming $\chi^{(2),film}_{zzx}=0$. We repeated our rotational measurement over a two photon spectral range of 2.6 to 3.4 eV at an angle of incidence of 65° to fit for $\chi^{(2),film}_{zzx}$ with the miscut angle fixed from the 15° rotational scan. We were unable to detect any strain or miscut induced nonlinearity within the limit of our measurement, and determined $\chi^{(2),film}_{zzx}<0.005\chi^{(2)}_{zxx}$. Figure 8 also displays $\chi^{(2),film}_{zzx}$.

Interface states that do not result from miscut induced strain are not observable by our rotational symmetry technique. These states could result from bonding between the substrate and the thin film.[53] Due to symmetry at the interface, these states most strongly affect $\chi^{(2)}_{zzz}$. Unfortunately, sample geometry precludes a direct measurement of this second-order susceptibility element.

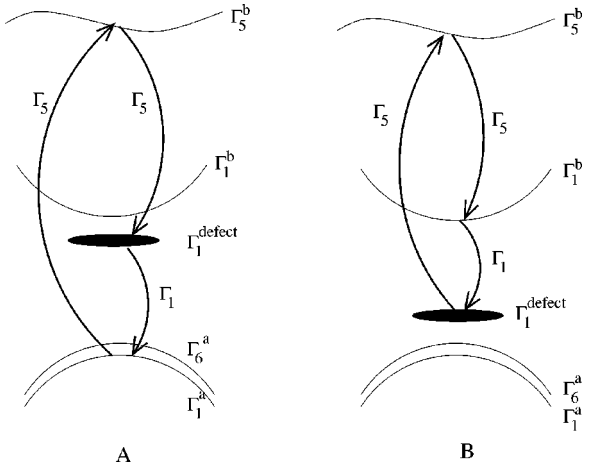

FIG. 10. Possible resonant three photon processes for the 2.80 eV resonance in $\chi^{(2)}_{zxx}$. (A) [(B)] represents a process that originates at the valence band (defect state). Only the bands that define the band gap and bands explicitly involved in the three-photon processes are displayed. (A) [(B)] corresponds to the first (second) entry in Table V.

IV. CONCLUSION

We have used second-harmonic generation to probe the bulk second-order nonlinear susceptibility elements of GaN over a two-photon energy range of 2.6–3.4 eV. We characterized the defect structure of our samples by photoluminescence and measured the index of refraction by a novel transmission method. Using various combinations of the fundamental and second-harmonic beams, we were able to separately measure both $\chi^{(2)}_{zxx}$ and $\chi^{(2)}_{xzx}$. Spectroscopy reveals a resonant enhancement in $\chi^{(2)}_{zxx}$ at a two-photon energy of 2.80 eV, which is absent in $\chi^{(2)}_{xzx}$. The subband gap enhancement is inconsistent with Miller's rule and may result from an intrinsic midgap defect state. In addition, we demonstrated sensitivity to the crystal miscut of GaN by rotational SHG, and we determined that the miscut strain does not induce forbidden bulk nonlinearities within our experimental limits ($\chi^{(2)}_{zzx}<0.005\chi^{(2)}_{zxx}$).

Finally, we developed new techniques for analyzing ultrafast second-harmonic generation. We employed zeroth-order and first-order expansions of the wave vectors with respect to angular frequency for the coefficients and phases, respectively. Group velocity mismatch is significant for SHG spectroscopy with ultrafast pulses in GaN samples as thin as 5 μm.

ACKNOWLEDGMENTS

We would like to thank E. J. Mele and M. S. Yeganeh for stimulating discussions. We thank J. L. P. Hughes and J. E. Sipe for providing us with their calculated nonlinear susceptibilities data. We would also like to thank C. S. Koeppen and A. F. Garito for technical help and for use of their facilities. A.G.Y. gratefully acknowledges the support of the NSF through Grant No. DMR-97-01657.

APPENDIX A: SECOND-HARMONIC GENERATION FROM A QUARTZ SLAB EXCITED BY AN ULTRAFAST LASER

In this appendix, we solve for the second-harmonic generation from a quartz slab excited by an ultrafast laser source. All of the approximations used in this appendix are also valid for SHG from GaN thin films. The fundamental field propagates from the vacuum to the nonlinear quartz crystal at $\mu=0$, where it generates a second-harmonic field. This field propagates through the crystal to the second crystal/vacuum interface at $y=d$. A second-harmonic field is transmitted through this interface and has a magnitude that depends on the boundary conditions. We solve for the transmitted SHG intensity using a first-order expansion with respect to $(\omega-2\omega_o)$ in the phase factors and a zeroth-order expansion in $(\omega-2\omega_o)$ for the multiplicative field coefficients. This model does not account for the effects of multiple reflections of the second-harmonic or fundamental fields. Even without incorporating these effects however, the model accurately captures both wave-vector mismatch and group velocity mismatch.

For bookkeeping purposes, we assume that our fundamental fields are labeled 1 and 2. This notation is used to explicitly exhibit the mixing of different frequency components of the same pulse in the SHG process. The form of the fundamental fields in angular frequency space is

$$\mathbf{E}_1(\mathbf{r},\omega_1)=\hat{x}\frac{\mathcal{E}_1}{2\pi}e^{ik(\omega_1)y}\exp\left(\frac{-4(\omega_1-\omega_o)^2}{\Delta\omega^2}\right) \quad \text{(A1)}$$

and

$$\mathbf{E}_2(\mathbf{r},\omega_2)=\hat{x}\frac{\mathcal{E}_2}{2\pi}e^{ik(\omega_2)y}\exp\left(\frac{-4(\omega_2-\omega_o)^2}{\Delta\omega^2}\right). \quad \text{(A2)}$$

The general expression that relates the second-order susceptibility to the fundamental fields is[54]

$$P_i^{(2)}(\omega)=4\pi^2\int_{-\infty}^{\infty}\int_{-\infty}^{\infty}\chi_{ijk}^{(2)}(\omega=\omega_1+\omega_2)E_j(\omega_1)\times E_k(\omega_2)\,\delta(\omega-(\omega_1+\omega_2))d\omega_1 d\omega_2. \quad \text{(A3)}$$

We can simplify this expression by expanding the phase of the fundamental fields to first order in $(\omega_1-\omega_o)$, i.e.,

$$k(\omega_1)=k_1^o+\frac{(\omega_1-\omega_o)}{v_{b_1}}, \quad \text{(A4)}$$

where

$$k_1^o=\frac{n(\omega_o)\omega_o}{c} \quad \text{and} \quad \frac{1}{v_{b_1}}=\left.\frac{\partial k}{\partial\omega_1}\right|_{\omega_o}. \quad \text{(A5)}$$

The subscript b denotes a bound wave. The second-order term in the expansion of $k(\omega_1)$ is responsible for the broadening of the pulse. Assuming a 130-fs fundamental pulse, we determined that the second-harmonic and fundamental pulses broaden less than 0.4% for a 5-μm film of GaN and less than 2×10^{-6} for a 3-mm slab of quartz over a range of frequencies probed in this experiment.[55] Thus, the first-order approximation is accurate. Using this first-order phase approximation, the nonlinear polarization is

$$P_x^{(2)}(r,\omega)=P_o e^{ik_b(\omega)y}\exp\left(\frac{-2(\omega-2\omega_o)^2}{\Delta\omega^2}\right) \quad \text{(A6)}$$

with

$$P_o=\frac{\sqrt{\pi}}{2\sqrt{2}}\Delta\omega\mathcal{E}^2\chi_{xxx}^{(2)}(\omega=2\omega_o). \quad \text{(A7)}$$

As expected, the nonlinear polarization has a Gaussian angular frequency distribution that is centered at $2\omega_o$. Note the use of the symbol $k_b(\omega)$ in the phase $P_x^{(2)}$. This symbol denotes that $k_b(\omega)$ is the bound wave vector, which has the functional form

$$k_b(\omega)=2k^o+\frac{(\omega-2\omega_o)}{v_b}. \quad \text{(A8)}$$

This is twice the wave vector of the fundamental field [Eq. (A4)]. We have assumed in this calculation that $\chi_{xxx}^{(2)}$ is a slowly varying function of frequency, assuming its center frequency value over the bandwidth of the pulse. Using Miller's rule, we calculated that $\chi_{xxx}^{(2)}$ varies less than 0.4% over the bandwidth of the Ti:Al_2O_3 laser pulse. Since the spectra of GaN varies slowly, this assumption is valid for GaN.

The second-harmonic fields may be calculated from the nonlinear wave equation and the nonlinear polarization. The nonlinear wave equation may be written in angular frequency space as

$$\left[\nabla\times(\nabla\times)-\frac{\epsilon(\omega)\omega^2}{c^2}\right]\mathbf{E}(\mathbf{r},\omega)=\frac{4\pi\omega^2}{c^2}\mathbf{P}^{(2)}(\mathbf{r},\omega). \quad \text{(A9)}$$

We assume that the bound wave solution (particular solution) to the nonlinear wave equation is

$$\mathbf{E_b}(\mathbf{r},\omega)=\hat{x}E_{bx}(\mathbf{r},\omega)=\hat{x}\zeta_b(\omega)e^{ik_b(\omega)y}. \quad \text{(A10)}$$

Thus, the wave equation simplifies to

$$\left[k_b^2(\omega)-\frac{\epsilon(\omega)\omega^2}{c^2}\right]E_{bx}(\mathbf{r},\omega)=\frac{4\pi\omega^2}{c^2}P_x^{(2)}(\mathbf{r},\omega). \quad \text{(A11)}$$

We simplify the equation further by assuming that the multiplicative coefficients of the field can be approximated by their zeroth order values, i.e.,

$$k_b^2(\omega) \approx \frac{4\epsilon_b \omega_o^2}{c^2} \tag{A12}$$

and

$$\frac{\epsilon(\omega)\omega^2}{c^2} \approx \frac{4\epsilon_f \omega_o^2}{c^2} \tag{A13}$$

with $\epsilon_b \equiv \epsilon(\omega_o)$ and $\epsilon_f \equiv \epsilon(2\omega_o)$. Thus, Eq. (A11) reduces to

$$E_{bx}(\omega) = \frac{4\pi P_x^{(2)}(\omega)}{\epsilon_b - \epsilon_f}. \tag{A14}$$

This relationship between the nonlinear polarization and the bound wave field is the same as for the monochromatic case. Although k_b^2 and $[\epsilon(\omega)\omega^2]/c^2$ vary over the pulse width, their difference is nearly constant. We calculated that this approximation introduces an error of less than 0.17% in the magnitude of the field.

We now consider the homogeneous solutions to the wave equation. These solutions are required to satisfy boundary conditions at both quartz/vacuum interfaces. There are four free wave fields: $\mathbf{E}_{f1}(\mathbf{r},\omega)$, which is generated at the first quartz/vacuum interface and traverses the quartz crystal, $\mathbf{E}_{f0}(\mathbf{r},\omega)$, which is reflected off of the first quartz/vacuum interface into the vacuum, $\mathbf{E}_{f1r}(\mathbf{r},\omega)$, which is reflected off of the second quartz/vacuum interface, and $\mathbf{E}_{f2}(\mathbf{r},\omega)$, which is the transmitted second-harmonic field. We assume that the fields have the form

$$\mathbf{E}_{fj}(\mathbf{r},\omega) = \hat{x}\zeta_{fj}(\omega)e^{\pm ik_{fj}(\omega)y}, \tag{A15}$$

where j is 1, $r1$, 0, or 2 and the sign of the phase is positive if the free wave propagates in the direction of the bound wave field or negative if it propagates in the direction opposite of the bound wave field. By applying continuity of the tangential components of the electric and magnetic fields at both $y=0$ and $y=d$, an expression for the transmitted free wave amplitude is determined as

$$\zeta_{f2}(\omega) = \frac{\zeta_{b1}(\omega)}{k_{f1}(\omega)+k_{f0}(\omega)}\Bigg[-2k_{f1}(\omega) \times\left(\frac{k_{b1}(\omega)+k_{f0}(\omega)}{k_{f1}(\omega)+k_{f0}(\omega)}\right)e^{i(k_{f1}(\omega)-k_{f0}(\omega)d} + [k_{b1}(\omega)+k_{f1}(\omega)]e^{i[k_{b1}(\omega)-k_{f0}(\omega)]d}\Bigg]. \tag{A16}$$

Using the zeroth-order approximation for the phases, the relationship between the angular frequency and the wave vector is

$$k_{f1}(\omega) = \frac{n_{f1}2\omega_o}{c} \quad \text{and} \quad k_{b1}(\omega) = \frac{n_{b1}2\omega_o}{c} \tag{A17}$$

with

$$n_{f1} \equiv n(2\omega_o) \quad \text{and} \quad n_{b1} \equiv n(\omega_o). \tag{A18}$$

This is the same approximation used in the simplification of the bound wave field. The transmitted wave envelope may be expressed as

$$\zeta_{f2}(\omega) = \alpha\zeta_{b1}(\omega)e^{i[k_{f1}(\omega)-k_{f0}(\omega)]d} + \beta\zeta_{b1}(\omega)e^{i[k_{b1}(\omega)-k_{f0}(\omega)]d}. \tag{A19}$$

with

$$\alpha = \frac{-2n_{f1}(n_{b1}+1)}{(n_{f1}+1)^2} \quad \text{and} \quad \beta = \frac{n_{b1}+n_{f1}}{n_{f1}+1}. \tag{A20}$$

By Fourier transforming the transmitted SHG field, $\mathbf{E}_{f2}(\mathbf{r},\omega)$, and using the first-order phase approximation again, the expressions in the text may be generated.

APPENDIX B: SECOND-HARMONIC GENERATION FROM GaN/Al_2O_3

In this appendix, we derive the SHG field transmitted through GaN/Al_2O_3 by boundary value techniques. We use the notation employed by Yeganeh *et al.*[33] to label our nonlinear fields. These fields are displayed in Fig. 5. The layers are denoted 0, 1, and 2 for air, GaN, and sapphire, respectively. Our model includes all fields that affect the magnitude of the transmitted intensity by at least 10%. For example, we assume no reflection of the linear light field, and hence, the bound wave field, from the GaN/Al_2O_3 interface. This assumption is valid because $|r_{12p}(\omega_o)|^2 < 0.015$, where $r_{12p}(\omega_o)$ is the Fresnel reflection coefficient for the p-polarized light at angular frequency ω_o with 1 (GaN) as the incident medium and 2 (sapphire) as the substrate medium. Although we ignore the reflection of linear light, we include the free wave field reflected from the GaN/Al_2O_3 interface. This field, E_{fr1}, is related to the free wave field, E_{f2}, that is generated at the GaN/Al_2O_3 interface and propagates through the sapphire substrate as $|E_{fr1}| \approx 0.1|E_{f2}|$.

The p-polarized fundamental light field generates a nonlinear polarization of the form

$$P_x^{(2)} = 2t_{p01}^2(\omega_o)\chi_{xzx}^{(2)}E_xE_z \tag{B1}$$

and

$$P_z^{(2)} = t_{p01}^2(\omega_o)(\chi_{zxx}^{(2)}E_xE_x + \chi_{zzz}^{(2)}E_zE_z). \tag{B2}$$

Note that E is the incident fundamental field and $t_{p01}(\omega_o)E$ is the fundamental field transmitted into the GaN film. The nonlinear polarization generated by an s-polarized fundamental field is

$$P_z^{(2)} = t_{s01}^2(\omega_o)\chi_{zyy}^{(2)}E_yE_y. \tag{B3}$$

The bound wave fields are determined by the nonlinear polarization, the nonlinear wave equation, and

$$\nabla\cdot\mathbf{E}_{b1} = \frac{-4\pi\nabla\cdot\mathbf{P}^{(2)}}{\epsilon_b}. \tag{B4}$$

The nonlinear bound wave fields are

$$E_{b1x} = \frac{4\pi}{\epsilon_b - \epsilon_f}\left[P_x^{(2)}\left(1-\frac{k_{b1x}^2}{k_{f1}^2}\right) - \frac{k_{b1x}k_{b1z}}{k_{f1}^2}P_z^{(2)}\right] \tag{B5}$$

and

$$E_{b1z}=\frac{4\pi}{\epsilon_b-\epsilon_f}\left[P_z^{(2)}\left(1-\frac{k_{b1z}^2}{k_{f1}^2}\right)-\frac{k_{b1x}k_{b1z}}{k_{f1}^2}P_x^{(2)}\right]. \quad \text{(B6)}$$

In order to satisfy boundary conditions, a free wave is generated at the air/GaN interface and propagates with the bound wave to the GaN/sapphire interface. This wave is

$$E_{f1}=\left(\frac{k_{f0}^2k_{f1z}}{k_{f0z}k_{f1}}-k_{f1}\right)^{-1}\left[\left(k_{b1z}-\frac{k_{f0}^2}{k_{f0z}}\right)E_{b1x}-k_{b1x}E_{b1z}\right]. \quad \text{(B7)}$$

At the GaN/sapphire interface, two additional free waves are generated: a field transmitted through the GaN/Al_2O_3 interface, E_{f2}, and a free wave reflected from the GaN/Al_2O_3 interface, E_{fr1}. These waves have the forms

$$E_{f2}=\left(\frac{k_{f1}^2k_{f2z}}{k_{f1z}k_{f2}}+k_{f2}\right)^{-1}\left[\left(k_{b1z}+\frac{k_{f1}^2}{k_{f1z}}\right)E_{b1x}e^{-ik_{b1z}d}-k_{b1x}E_{b1z}e^{-ik_{b1z}d}+2k_{f1}E_{f1}e^{-ik_{f1z}d}\right] \quad \text{(B8)}$$

and

$$E_{f1r}=-\left(\frac{k_{f2}^2k_{f1z}}{k_{f2z}k_{f1}}+k_{f1}\right)^{-1}\left[\left(k_{b1z}-\frac{k_{f2}^2}{k_{f2z}}\right)E_{b1x}e^{-ik_{b1z}d}-k_{b1x}E_{b1z}e^{-ik_{b1z}d}+\left(k_{f1}-\frac{k_{f2}^2k_{f1z}}{k_{f2z}k_{f1}}\right)E_{f1}e^{-ik_{f1z}d}\right]. \quad \text{(B9)}$$

Therefore, the field transmitted through GaN/Al_2O_3 is

$$\mathbf{E}_t(\mathbf{r},2\omega_o)=\hat{e}t_{p20}(2\omega_o)(E_{f2}e^{ik_{f2}\Delta}+r_{p10}(2\omega_o)t_{p12}(\omega_o)E_{f1r}e^{ik_{f1}\delta}) \quad \text{(B10)}$$

with

$$\delta=\frac{2d}{\cos\theta_{f1}} \quad \text{(B11)}$$

and

$$\Delta=2d\tan\theta_{f1}\sin\theta_{f1}. \quad \text{(B12)}$$

Note that δ is the round-trip distance that E_{f1r} travels in the GaN film and Δ is the distance that E_{f2} travels in the sapphire substrate during the round trip of E_{f1r}. Equation (B10) is rewritten in the text as Eqs. (25) and (32) to explicitly demonstrate the transmitted wave's dependence on the nonlinear susceptibilities of GaN, the applied linear fields, and propagation effects.

Equation (B10) does not include the effect of the ''walk off'' between the bound and free waves. Walk off refers to the spatial separation of the bound and free waves that results from different directions of propagation of these waves in the nonlinear crystal. Walk off decreases the overlap of the bound and free waves, and hence modifies the interference of these waves. For an 800-nm beam with an angle of incidence θ_0 of 46.0°, the corresponding free and bound waves propagate in GaN with angles of $\theta_{f1}=16.4°$ and $\theta_{b1}=18.0°$, respectively. After propagating through 5 μm of GaN, the spatial separation of the center of the free and the bound waves is 0.15 μm. Therefore, walk off is insignificant in our experiment. In addition, no walk off occurs in our SHG measurements of quartz because $\theta_b=0°$ and $\theta_f=0°$.

[1] J. L. P. Hughes, Y. Wang, and J. E. Sipe, Phys. Rev. B **55**, 13 630 (1997).

[2] R. Zhang, K. Yang, L. H. Qin, H. T. Shi, Y. Shi, S. L. Gu, Y. D. Zheng, Z. C. Huang, and J. C. Chen, J. Vac. Sci. Technol. A **14**, 840 (1996).

[3] M. O. Manasreh, Phys. Rev. B **53**, 16 425 (1996).

[4] P. Kung, C. J. Sun, A. Saxler, H. Ohsato, and M. Razeghi, J. Appl. Phys. **75**, 4515 (1994).

[5] W. Shan, T. Schmidt, X. H. Yang, J. J. Song, and B. Goldenberg, J. Appl. Phys. **79**, 3691 (1996).

[6] K. Hiramatsu, T. Detchprohm, and I. Akasaki, Jpn. J. Appl. Phys. Part 1 **32**, 1528 (1993).

[7] S. Nakamura, M. Senoh, S.-I. Nagahama, N. Iwasa, T. Yamada, T. Matsushita, H. Kiyoku, Y. Sugimoto, T. Kozaki, H. Umemoto, M. Sano, and K. Chocho, Appl. Phys. Lett. **72**, 211 (1998).

[8] T. Ishidate, K. Inoue, and M. Aoki, Jpn. J. Appl. Phys. **19**, 1641 (1980).

[9] I. M. Catalano, A. Cingolani, M. Lugara, and A. Minafra, Opt. Commun. **23**, 419 (1977).

[10] J. Miragliotta, D. K. Wickenden, T. J. Kistemacher, and W. A. Bryden, J. Opt. Soc. Am. B **10**, 1447 (1993).

[11] J. Miragliotta, W. A. Bryden, T. J. Kistenmacher, and D. K. Wickenden, in *Diamond, SiC and Nitride Wide Bandgap Semiconductors*, edited by C. H. Carter, G. Gildenblat, S. Nakamura, and R. J. Nemanich, MRS Symposia Proceedings No. 339 (Materials Research Society, Pittsburgh, 1994), p. 583.

[12] H. Y. Zhang, X. H. He, Y. H. Shih, M. Schurman, Z. C. Feng, and R. A. Stall, Appl. Phys. Lett. **69**, 2953 (1996).

[13] M. A. Khan, J. N. Kuznia, J. M. Van Hove, D. T. Olson, S. Krishnankutty, and R. N. Kolbas, Appl. Phys. Lett. **58**, 526 (1991).

[14] D. Brunner, H. Angerer, E. Bustarret, F. Freudenberg, R. Höpler, R. Dimitrov, O. Ambacher, and M. Stutzman, J. Appl. Phys. **82**, 5090 (1997).

[15] W. P. Lin, P. M. Lundquist, G. K. Wong, E. D. Rippert, and J. B. Ketterson, Appl. Phys. Lett. **63**, 2875 (1993).

[16] E. Ejder, Phys. Status Solidi A **6**, 445 (1971).

[17] G. Yu, G. Wang, H. Ishikawa, M. Umeno, T. Soga, T. Egawa, J. Watanabe, and T. Jimbo, Appl. Phys. Lett. **70**, 3209 (1997).

[18] See, for example, J. A. Dobrowolski, in *Handbook of Optics*, edited by Michael Bass (McGraw Hill, New York, 1995); H. A. Macleod, in *Thin-Film Optical Filters* (Elsevier, New York, 1969).

[19] W. E. Angerer, Ph.D. thesis, University of Pennsylvania, Philadelphia, 1998.

[20] I. H. Malitson, J. Opt. Soc. Am. **52**, 1377 (1962).
[21] R. Dingle and M. Ilegems, Solid State Commun. **9**, 175 (1971).
[22] W. Rieger, R. Dimitrov, D. Brunner, E. Rohrer, O. Ambacher, and M. Stutzmann, Phys. Rev. B **54**, 17 596 (1996).
[23] M. R. H. Khan, Y. Ohshita, N. Sawaki, and I. Akasaki, Solid State Commun. **57**, 405 (1986).
[24] B. K. Meyer, D. Volm, A. Graber, H. C. Alt, T. Detchprohm, A. Amano, and I. Akasaki, Solid State Commun. **95**, 597 (1995).
[25] T. Matsumoto and M. Aoki, Jpn. J. Appl. Phys. **13**, 1804 (1974).
[26] S. Fischer, C. Wetzel, E. E. Haller, and B. K. Meyer, Appl. Phys. Lett. **67**, 1298 (1995).
[27] J. Neugebauer and C. G. Van de Walle, Appl. Phys. Lett. **69**, 503 (1996).
[28] E. Calleja, F. J. Sánchez, D. Basak, M. A. Sánchez-García, E. Muñoz, I. Izpura, F. Calle, J. M. G. Tijero, J. L. Sánchez-Rojas, B. Beaumont, P. Lorenzini, and P. Gibart, Phys. Rev. B **55**, 4689 (1997).
[29] E. F. Schubert, I. D. Goepfert, and J. M. Redwing, Appl. Phys. Lett. **71**, 3224 (1997).
[30] M. S. Yeganeh, J. Qi, J. P. Culver, A. G. Yodh, and M. C. Tamargo, Phys. Rev. B **49**, 11 196 (1994).
[31] P. D. Maker, R. W. Terhune, M. Nisenoff, and C. M. Savage, Phys. Rev. Lett. **8**, 21 (1962).
[32] N. Bloembergen and P. S. Pershan, Phys. Rev. **128**, 606 (1962).
[33] M. S. Yeganeh, J. Qi, J. P. Culver, A. G. Yodh, and M. C. Tamargo, Phys. Rev. B **46**, 1603 (1992).
[34] J. Comly and E. Garmire, Appl. Phys. Lett. **12**, 7 (1968).
[35] S. A. Akhmanov, A. S. Chirkin, K. N. Drabovich, A. I. Kovrigin, R. V. Khokhlov, and A. P. Sukhorukov, IEEE J. Quantum Electron. **QE-4**, 598 (1968).
[36] L. B. Zhang, H. R. Choo, and M. C. Downer, Appl. Opt. **29**, 3927 (1990).
[37] I. V. Tomov, R. Fedosejevs, and A. A. Offenberger, IEEE J. Quantum Electron. **QE-18**, 2048 (1982).
[38] W. H. Glenn, IEEE J. Quantum Electron. **QE-5**, 284 (1969).
[39] H. W. K. Tom, T. F. Heinz, and Y. R. Shen, Phys. Rev. Lett. **51**, 1983 (1983).
[40] The sapphire miscut induces a rotationally dependent birefringence that rotates the *p*-polarized SHG light into the *s*-polarized direction. Thus, in the *s*-out polarization, both *s*-polarized SHG, which results from the GaN miscut, and *p*-polarized SHG, which results from the sapphire miscut, are measured. Both of these effects have (to lowest order in α) a crystal orientation dependence of $\sin\phi$.
[41] J. Chen, Z. H. Levine, and J. W. Wilkins, Appl. Phys. Lett. **66**, 1129 (1995).
[42] R. C. Miller, Appl. Phys. Lett. **5**, 17 (1964).
[43] B. F. Levine, Phys. Rev. B **7**, 2600 (1973).
[44] Y. R. Shen, *The Principles of Nonlinear Optics* (Wiley, New York, 1984).
[45] S. Strite and H. Morkoç, J. Vac. Sci. Technol. B **10**, 1237 (1992).
[46] D. W. Jenkins and J. D. Dow, Phys. Rev. B **39**, 3317 (1989).
[47] See, for example, C. F. Klingshirn, in *Semiconductor Optics* (Springer-Verlag, Berlin 1995).
[48] S. Bloom, G. Harbeke, E. Meier, and I. B. Ortenburger, Phys. Status Solidi B **66**, 161 (1974).
[49] W. Daum, H.-J. Krause, U. Reichel, and H. Ibach, Phys. Scr. **T49**, 513 (1993).
[50] C. Meyer, G. Lüpke, U. Emmerichs, F. Wolter, H. Kurz, C. H. Bjorkman, and G. Lucovsky, Phys. Rev. Lett. **74**, 3001 (1995).
[51] M. S. Yeganeh, J. Qi, A. G. Yodh, and M. C. Tamargo, J. Opt. Soc. Am. B **10**, 2093 (1993).
[52] This coordinate system has a mirror plane in the *xz* plane. Therefore, susceptibility elements such as $\chi^{(2)}_{zzy}$ and $\chi^{(2)}_{yzz}$ are forbidden.
[53] T. F. Heinz, F. J. Himpsel, E. Palange, and E. Burstein, Phys. Rev. Lett. **63**, 644 (1989).
[54] A. C. Newell and J. V. Moloney, *Nonlinear Optics* (Addison-Wesley, Redwood City, California, 1992).
[55] S. De Silverstri, P. Laporta, and O. Svelto, IEEE J. Quantum Electron. **QE-20**, 533 (1984).